Spectrochimica Acta Part B 167 (2020) 105852

Contents lists available at ScienceDirect

Spectrochimica Acta Part B

journal homepage: www.elsevier.com/locate/sab

Experimental evaluation of the in-the-field capabilities of total-reflection X-ray fluorescence analysis to trace fine and ultrafine aerosol particles in populated areas

János Osán[a,*], Endre Börcsök[a], Ottó Czömpöly[a], Csenge Dian[a,b], Veronika Groma[a], Luca Stabile[c], Szabina Török[a]

[a] Environmental Physics Department, Centre for Energy Research, Konkoly-Thege M. út 29-33., 1121 Budapest, Hungary
[b] Department of Meteorology, Eötvös Loránd University, Pázmány Péter st. 1/A, 1117 Budapest, Hungary
[c] Department of Civil and Mechanical Engineering, University of Cassino and Southern Lazio, 03043 Cassino, Italy

ARTICLE INFO

Keywords:
Atmospheric aerosols
Ultrafine particles
Cascade impactor
TXRF
Elemental size distribution

ABSTRACT

European countries have made progress in reducing particulate air pollution in recent decades being concerned about their heath and climate effect. In addition to determining particulate number size distributions, it is crucial to have a methodology to determine size distribution of elemental concentrations down to the ultrafine size fraction. The present study shows capabilities for combination of May-type cascade impactor sampling and laboratory total-reflection X-ray fluorescence analysis on ambient aerosol samples taken in urban areas of Budapest (Hungary) and Cassino (Italy). In addition, results for a sample collected in Budapest during the fireworks provided for the Hungarian National Day are discussed.

The combined novel method is suitable for determining size distributions for major and trace elemental concentrations form ultrafine to coarse particles (70 nm up to 10 μm) in seven size fractions. Moreover, short sampling times (1–4 h) are sufficient for reaching detection limits in the range of 100 pg/m^3 for transition metals. The size and time resolution were found to be optimal for identifying pollution episodes with elevated elemental concentrations. The in-the-field analytical applicability of the proposed method for major and trace elements is demonstrated by comparison to elemental size distributions resulted from destructive analytical techniques.

1. Introduction

Ambient aerosol particles (particulate matter – PM) are among the most harmful atmospheric pollutants in highly populated areas. Origin of these particles is human, industrial and natural processes. Large fraction of anthropogenic particles come from combustion of fossil fuels for domestic heating, traffic and industrial purposes. Concentration of aerosols is highest in the northern hemisphere with industrial activity. Impact of PM pollution in urban areas exceeds in many countries the World Health Organization (WHO) air quality guideline concentrations. In Europe, population of Southern, Central and Eastern Europe is suffering most of the exceedances [1]. Many Italian cities mostly in the Po valley have very high PM concentrations, while Warsaw, Sofia and Istanbul were European cities with the highest PM pollution level in 2017. Many previous studies concentrated in defining the sources and their contribution to the PM concentrations to find efficient tools to reduce emissions [2]. Most approaches that are frequently used for source profiling need long sampling times, an extended set of analytical techniques that include measurement of major and trace elements as well as special organic marker components in the aerosol. A recent epidemiological study has shown that short term exposure to elevated concentration of ambient PM might trigger acute effects like hart rate variability [3], especially fine ($PM_{2.5}$) and ultrafine ($PM_{0.1}$) particles, where PM_x denotes particulate matter with equivalent aerodynamic diameter less than x μm. Submicron particles got special attention recently due to the evidence of their detrimental health effect. For epidemiological studies analytical techniques based on table-top non-portable instrumentation having very low time resolution (daily) do not result in suitable data for exposure-response function since human activity changes more rapidly. The daily average of monitoring stations is not a representative input value for such studies since people usually spend much less time (ground travel, recreation in city parks) outdoors

* Corresponding author.
E-mail address: janos.osan@energia.mta.hu (J. Osán).

https://doi.org/10.1016/j.sab.2020.105852
Received 28 February 2020; Received in revised form 1 April 2020; Accepted 2 April 2020
Available online 05 April 2020

where the emission sources and atmospheric conditions are rapidly changing. Emission of submicron particles can be very short-term and can relate to the traffic flow [4]. It is well known that the size distribution of elemental concentrations has a time variation dependent on sources and meteorological conditions. In order to have a reliable estimation of health effects of the inhaled particles and their source contributions, information on size-resolved chemical composition of aerosol particles with sufficient time resolution is imperative.

With the emergence of particle spectrometers capable of determining size distribution of submicron particles with a high counting efficiency for ultrafine particles, several groups have studied the number size distribution using scanning mobility particle sizers (SMPS) to attribute ultrafine particle sources. Although SMPS has a very high size and time resolution, it does not provide information on the chemical composition of particles.

Quantitative analysis of elements present in ng/m^3 in aerosol size fractions poses difficult task for routine measurement of large sample numbers related to short sampling times that are necessary for epidemiologically relevant time resolution. On line real time measurement resulting in simultaneous size and composition data is only possible by single particle analysis by various mass spectrometry (single-particle aerosol mass spectrometry - SPAMS or aerosol time-of-flight mass spectrometry - ATOFMS) [5]. Since the first of such commercial instruments a lot of technical improvements happened, the analytical technique became very useful for organic compounds in particles larger than 200 nm up to 2.5 μm, with an inherently high size resolution [6]. Detection limits allow determination of major and minor compounds in individual particles. Real-time measurement has the advantage to avoid sampling artifacts, degradation or reaction of analytes during storage.

Off-line sampling with impactors allows cost-effective pre-concentration of the analytes and enables real trace analysis with various techniques. Typical approach for mass size distribution of chemical elements or compounds consists of sampling onto filters or Al plates in cascade impactors, followed by leaching or digestion and ion chromatography (IC), atomic absorption spectrometry (AAS) or inductively coupled plasma optical emission spectrometry / mass spectrometry ICP-OES / ICP-MS) analysis. A wide range of cascade impactors of different size resolution (3 to 14 stages) and different deposition pattern was applied for this task. With these techniques a maximum time resolution of 12 h was reached [7,8], but typically 24 h–72 h sampling was performed, resulting in 10–100 m^3 aerosol collected per sample. For a typical 24-h (24 m^3) sample on one single impactor stage, detection limits in the ng/m^3 range were reported for IC for major water soluble ions [9,10], and for ICP-OES for metallic elements [11]. Using ICP-MS, detection limits of 1–10 pg/m^3 or even below could be reached [12,13]. Applications of non-destructive X-ray fluorescence (XRF) techniques on analysis of filters loaded to impactor stages were also reported, with detection limits of 1–30 ng/m^3 for both energy-dispersive [14,15], and wavelength-dispersive XRF [16] for 24-h samples. Elemental size distributions obtained by XRF should be considered carefully due to the non-homogeneous deposition of particles on the impactor plates.

An increased time resolution of a few hours can be reached when a limited size resolution (only 3 stages) is applied as typically used in rotating drum impactors (RDI) or streaker samplers, but due to the sharp and close-lying strips of deposited particles a method with small beam size and high efficiency (particle-induced X-ray emission - PIXE or synchrotron radiation XRF - SRXRF) is necessary [17,18]. Applying RDI with high size resolution (8 stages covering the range of 0.07 to 10 μm) a continuous sampling at a 3-h time resolution became possible but the elemental analysis requires orders of magnitude higher X-ray fluxes available only at SR sources [19]. SRXRF was recently applied to cascade impactor samples with 6-h time resolution with special emphasis on quasi-ultrafine particles [20]. Work of users at such research infrastructure is available for twice a few days per year at best.

A promising alternative for elemental analysis of aerosol samples is total-reflection X-ray fluorescence analysis (TXRF). This technique is well suited for analysis of dried residues of solutions pipetted onto flat, totally reflecting surfaces. The most common way for TXRF analysis of airborne PM samples of filters is acid digestion and measurement as a liquid sample [21]. A small portion of the deposited filter area can also be transferred to the center of the reflector followed by removal of the filter material by cold plasma ashing [22]. If reflectors are used as collection surfaces in cascade impactors, the deposited particles can be analyzed by TXRF directly [23] or after cold plasma ashing depending on the pre-treatment of collection substrates [24,25]. However, the usually inhomogeneous deposition pattern on the impactor plates should be carefully considered. To date, studies reported on combination cascade impactor sampling and laboratory TXRF analysis involve low time [22] or size [24] resolution.

This paper aims to demonstrate capabilities of combination of May impactor sampling and laboratory TXRF for determination of size distribution of selected elements in a wide diameter range involving part of ultrafine particles. Sampling on Si wafers enables further non-destructive analysis by scanning electron microscopy (SEM), Raman spectroscopy or X-ray absorption spectrometry (XAS) [26]. Results for two European locations in different atmospheric pollution episodes are discussed as application examples. Size distributions of major and trace elements obtained in the present study are compared to those determined using IC and ICP-MS / ICP-OES after leaching or digestion of aerosol particles collected onto filters by different cascade impactors.

2. Materials and methods

2.1. Sampling and on-site monitoring

Sample sets selected for the present study were collected from three campaigns at two cities, Cassino, Central Italy, 20–27 September 2018; and Budapest, Hungary, 31 July – 09 August 2019 and 20 August 2019.

2.1.1. Cassino, 20–27 September 2018

The sampling site is a covered balcony (floor surface 3.9 m × 7.5 m) on the second floor of a building owned by the University of Cassino and Southern Lazio. The building is placed in the urban area of Cassino (Central Italy, 30 km from the Tyrrhenian Sea, resident population 33,000 inhabitants; surface area 83 km^2) and flanks a two-ways single-lane street with free flow traffic conditions characterized by a traffic density of 24 ± 3 vehicles min^{-1} with a mean velocity of about 30–40 km h^{-1} [27]. The street can be considered a wide canyon characterized by large openings on the walls. The sampling site (covered balcony) is placed at a distance of < 20 m from the street. The sampling point is at about 400 m from the fixed sampling monitoring station of the regional Environmental Protection Agency.

The weather conditions in Cassino during the measurement campaign were obtained from the fixed sampling monitoring station of regional Environmental Protection Agency. During the campaign the precipitations were negligible, but slightly different meteo-climatic conditions were detected before and after 25 September 2018 as a cold front was moving through the area at that time. In particular, in the period 21–24 Sept 2018 the average temperature and relative humidity were equal to 24.9 °C and 72.2%, respectively, and the wind prevalent direction was South with a median speed of 0.7 m/s. On the contrary, on period 25–27 Sept 2018, lower average temperature and relative humidity values were measured (19.5 °C and 47.1%, respectively) as well as the wind condition changed, indeed, different prevalent directions were recognized (S, NW, E) with a slightly higher median speed (about 1.0 m/s). Due to this variation in the meteo-climatic conditions, a decrease in the 24-h average PM_{10} concentrations measured by the Environmental Protection Agency at the fixed sampling point was detected in the period 25–27 Sept 2018 (average value of 12.3 μg/m^3 with respect to 22.4 μg/m^3 measured on 21–24 Sept 2018).

2.1.2. Budapest, 31 July – 09 August 2019

The sampling site is a covered balcony (floor surface 3 m × 1.5 m) on the first floor of a building not far from a traffic center in Budapest, Hungary (47°28′46″N, 19°02′37″E). The measurement site is located in a green belt residential area, 15 m far from a one-way side street which serves little traffic (1500 cars·day^{-1}). However, it is situated 300 m close to a double-lane street with approximately 7000 cars on weekdays. A monitoring station of Hungarian Air Quality Network operates about 500 m far from sampling point.

During the measurement campaign, mostly variable moisture content and unstable air mass determined the weather of the Carpathian Basin. However, only traceable amount of precipitation was detected at measurement site on the 2 and 6 August. Warmer air mass arrived over the Carpathian Basin from 5 to 7 August from Western Europe, but on the night of 7 August, a cold front crossed over. The daily average temperature was 20–26 °C and the maximum temperature was 26–31 °C in Budapest in this period. During the overall campaign, the median of wind speed was 2.4 ms^{-1}, light breeze periods were detected only on 1 and 3 August. Prevailing wind direction was NW nearly in the entire period, except on 7 August, when due to the cold front, the characteristic wind direction was SW.

2.1.3. Budapest, 20 August 2019, firework sampling

The sampling site is at the heart of Budapest, close to the Széchenyi Chain Bridge on Pest side. Samples were collected from a window at ground floor looking in the direction of Danube from the main building of Hungarian Academy of Sciences. The fireworks were launched from the Széchenyi Chain Bridge and from boats on river Danube, which were at a distance less than 400 m. This area is the most popular for observing the 20th August firework between roughly half a million people who attends the riverside every year for admiring the 30 min long event. On 20 August 2019, a front approached the Carpathian Basin from Western Europe. The weather was sunny and warm without precipitation.

2.1.4. Size-fractionated sampling

A 9-stage extension of the May-type cascade impactor [28] was used for size-fractionated sampling of aerosol particles. At a flow rate of 16.7 L/min, the 9-stage May-impactor has aerodynamic cut-off diameters of 17.9, 8.9, 4.5, 2.25, 1.13, 0.57, 0.29, 0.18 and 0.07 μm, for stages 1 to 9, respectively. In order to cover close to the whole PM_{10} range, samples were collected on stages 3 to 9, on 20 × 20 mm^2 Si wafers. In the May-type cascade impactor, the jets are slits of 50 mm length and widths decreasing with increasing stage number, resulting in deposition pattern of aerosol particles as thin stripes of 0.1 mm (stage 9) to 1 mm (stage 3) width.

As the collected samples were intended to be available for different (micro)analytical investigations, no pre-treatment of the Si surfaces was performed, however, the sample collection time was kept short in order to minimize bounce-off of particles. Samples presented in this study were typically collected for 4 h, ranging from 1 to 6 h.

2.1.5. On-site monitoring

During the campaigns except the firework sampling, airborne particulate monitoring devices were operated on-site. The total PM_{10} mass concentration was measured using a Tapered Element Oscillating Microbalance (TEOM, Series 1400a, Thermo Fisher, Franklin, MA, USA) at a 30-min resolution.

The black carbon (BC) content of aerosol particles was determined with a portable aethalometer (AE42–7, Magee Scientific, USA), in a 2-min time resolution. The instrument collects aerosol particles on a filter continuously by drawing air through the filter. A light source irradiates the filter at seven different wavelengths (370 to 950 nm) and two detectors measure the transmission of light through the filter tape containing the sample and through an unloaded reference area of the filter. BC concentration is calculated using internal calibration based on attenuation measurements at 880 nm wavelength. Concentrations are recorded as BC-equivalent for all seven wavelengths, giving opportunity to study the wavelength dependence of optical attenuation of aerosol particles. Attenuation in the near-ultraviolet at 370 nm has a great sensitivity to aromatic organic species such as are found in tobacco smoke, wood fire smoke. A compensation correction was executed based on the model of Weingartner et al. [29] to avoid the systematic errors caused by loading effects.

2.2. Total-reflection X-ray fluorescence (TXRF)

A compact TXRF system [30] comprising a low-power X-ray tube, a multilayer monochromator and a modified WOBI-module attachment [31] was applied for the present study. The sample plane is defined by three steel balls with arrangement allowing measurement of 20 × 20 mm^2 reflectors in addition to standard 30-mm diameter discs. A 50-W microfocus Mo-anode X-ray tube (Petrick, Bad Blankenburg, Germany) was operated at 50 kV and 1 mA, and Mo-Kα X-rays were selected for excitation using a Mo/Si multilayer monochromator (AXO, Dresden, Germany). The beam profile was defined by two slits of 100 μm × 10 mm, the first one mounted directly in front of the beam exit of the X-ray tube, while the second, adjustable one after the multilayer monochromator [32,33]. A 7-mm^2 silicon drift detector (KETEK, Munich, Germany) with a round Zr collimator and an analogue signal processing unit (PGT, Princeton, USA) were used to record X-ray spectra. Typically 3000 s counting time was used for Si wafers with moderate load of aerosol particles. Measurements were performed in air.

Si wafer squares were analyzed with aerosol deposit stripes horizontally, perpendicular to the beam direction and parallel to the slit defining the line-shaped beam. X-ray spectra were evaluated using the AXIL software [34]. Due to the fact that the aerosol particles are deposited as a stripe, the usual internal standardization using a droplet from single-element solution (Ga or Y) is not straightforward and would cause disturbances for the other non-destructive techniques. For this reason, quantification of elemental content in ng/sample (i.e. ng of elemental mass along the total 20 mm stripe) was performed using calibration based on external standards. Calibration standards were prepared on Si wafers from a multielemental standard solution (Merck IV, 23 elements). Linear arrays of droplets were deposited with a 1-mm spacing on the centerline of the wafers along the full length of 20 mm by a nanoliter injector (WPI, USA). These standard samples were used for determining the sensitivities relative to chromium, listed in Table 1. The absolute mass was calibrated using standard Si chips of identical dimensions to samples, containing 4 ng and 8 ng (± 5%) Cr in the form of 2.7 μm diameter pads of respectively 50 nm and 100 nm height arranged in seven rows along the centerline of the square in a 350 μm wide stripe [35,36]. As the pads are horizontally microscopic in dimension, they are suitable for quantitation of coarser micron-size particles as well. Angular scans on the Cr chips with structures of 50 nm and 100 nm height showed profiles similar to those for microparticles sitting on a flat surface (nearly constant double Cr-Kα intensity below the critical angle with respect to the Cr-Kα intensity above the critical angle) proving their suitability as standards in a wide particulate diameter range [35,36]. Since the Si wafers are placed in the impactor in a ± 100 μm precision, the geometry of the deposited aerosol particles can be considered as the same. The homogeneity of the particulate deposit along the stripe was previously tested using synchrotron-radiation TXRF [37] and found to be within 3%. The respective atmospheric concentrations were calculated for each size fraction of each sample considering the total length of deposited stripes (50 mm for each impactor stage) and the collected air volume.

Table 1
Relative sensitivities and detection limits for elements K—Sr (based on Kα X-rays), Ba and Pb (based on Lα line) from a deposited particulate stripe of a single impactor stage from 1 m^3 sampled air measured by TXRF (50 kV, 1 mA, 3000 s, Mo-Kα excitation).

Element	Analytical line	Relative sensitivity (S_{Cr} = 1)	Detection limit (ng/m^3)
S	Kα	0.12	7.2
Cl	Kα	0.26	2.9
K	Kα	0.43	1.9
Ca	Kα	0.50	1.7
Ti	Kα	0.69	1.2
Cr	Kα	1.00	0.69
Mn	Kα	1.22	0.70
Fe	Kα	1.48	0.39
Ni	Kα	2.11	0.24
Cu	Kα	2.47	0.19
Zn	Kα	2.84	0.15
As	Kα	3.83	0.09
Se	Kα	4.05	0.09
Br	Kα	4.17	0.09
Sr	Kα	3.59	0.11
Ba	Lα	0.22	3.8
Pb	Lα	1.69	0.20

3. Results and discussion

3.1. Analytical capabilities of TXRF for May-impactor samples

Detection limits for elements K—Sr, Ba and Pb determined for one particle size fraction collected onto a Si wafer from 1 m^3 air measured by TXRF for 3000 s are shown in Table 1, along with elemental sensitivities relative to chromium. For transition metals and Pb, detection limits lower than 1 ng/m^3 can be reached that are well below the limit values (as yearly averages) for Ni (20 ng/m^3), As (6 ng/m^3) and Pb (500 ng/m^3) as stated in EU regulations. According to US EPA NAAQS Tables, however, the limit value for lead (as 3 month rolling average) is lower, 150 ng/m^3. The detection limits for a single stage (size fraction) are three times higher than those reported by Prost et al. [25], mainly due to the different detector solid angle (7 mm^2 vs 80 mm^2). It should also be noted that the higher size resolution (9 stages vs 3 stages) results in a lower mass of aerosol collected from a unit air volume at an individual stage.

Since internal standardization using liquid droplets is inconvenient for stripe-like deposition, a quantification approach based on external standards was used. However, without internal standard the repeatability of the measurement geometry is of high importance and accounts for a major part of the uncertainty burden in addition to the uncertainty of the calibration itself.

In order to test the repeatability, four samples loaded with particulate matter containing different elements (from S to Bi) at different mass levels were measured ten times by two operators (five times at the same position and five times rotated by 180°, but always unloaded and reinserted again). Results are presented as relative standard deviation of peak areas from the 10 measurements, plotted versus the peak area itself (Fig. 1a) as well as peak-to-background ratio (Fig. 1b).

It can be seen in Fig. 1a that the overall repeatability precision is always worse than the counting statistics and remains between 3 and 5% for peak areas greater than 10,000 counts. For peaks with more than 1000 counts, the repeatability precision is better than 8%. The precision worsens to around 15% for peak areas down to 250 counts. Smaller area peaks with peak-to-background ratios less than one (see Fig. 1b) encounter the highest relative standard deviation, 20–31%.

The long-time stability of the system (beam profile, sample and detector geometry) was also tested by measurements of a wafer with a linear arrays of droplet residues of multielement standard (containing 20 ng of each element along the 20 mm width of the square) in regular intervals. The variation of the X-ray intensity was within 3–5% in a one-year period monitored.

These findings indicate that a moderate precision of < 15% can be reached with quantification without using internal standardization. This precision is sufficient to show differences in elemental size distributions based on concentrations determined by TXRF for each size fraction.

3.2. Elemental size distributions

In order to show the capability of the developed impactor TXRF elemental analysis for aerosol research, analytical data are discussed for ambient aerosol sampling campaigns at Cassino and in Budapest. Finally the potential for an event with a short time emission (< 0.5 h) as a proxy of forensic study is shown during fireworks of Budapest National Day. Although all sample sets (several hundreds of Si wafers) were analyzed by TXRF, results for seven sample sets related to different pollution episodes and meteorological circumstances are discussed (Table 2). Samples were selected for interesting events showing applicability of the method for aerosol chemistry.

In line with the expected lognormal distribution, size distributions of atmospheric elemental masses are presented as $\Delta C/\Delta \log d$ in ng/m^3, calculated from air concentrations C for each size fraction determined by TXRF. Since the argument of the log function must be dimensionless, d denotes relative particle diameter ($d = d_p/d_{ref}$, where d_p is the particle diameter and d_{ref} = 1 μm). The discrete values for the cascade impactor stages are plotted at the representative diameter, i.e. geometrical average of the lower and upper cut-off diameters for each stage. The size distribution of elemental concentrations for the selected samples collected at Cassino and in Budapest are shown in Figs. 2 and 3.

3.2.1. Pollution episodes at Cassino and in Budapest

At Cassino, the ambient air mass with high concentration of PM including carbonaceous aerosols present before the meteorological front was removed from the sampling site and replaced by air mass of mainly marine origin. In the sample from Cassino after meteorological front (25 September 2018, sample CM08), the total *chlorine* concentration (in PM_9, sum for May impactor stages 3–9) was 340 (± 20) ng/m^3 and the size distribution (Fig. 2) shows that Cl was present in the coarse mode (main diameter range 2–10 μm) as expected for sea salt aerosols. The size distribution obtained by cascade impactor sampling and TXRF is consistent with IC measurements for Cl^- from 160-h size-fractionated samples influenced by marine air masses [10], showing that the combined method provides realistic results for impactor stages covering the coarse fraction.

Sulfur is the representative element for secondary sulfate aerosols that are formed from gaseous pollutants through nucleation and accumulation, consisting mainly of ammonium sulfate and secondary organic sulfate particles. These particles are in the fine fraction that can be subdivided to ultrafine, condensation (main diameter range 0.15–0.6 μm) and droplet modes (main diameter range 0.5–2 μm). The modal diameter of sulfate has seasonal and geographical variation between 0.2 and 0.7 μm, as obtained through IC measurements of SO_4^{2-} in size fractionated samples for long collection times [10,38]. It was found to be generally the smallest for summertime rural aerosols [38]. The air mass at Cassino before the meteorological front (21 September 2018, sample CM03) had high concentration of traffic and long-range transport related particles. It can be highlighted from Fig. 2 that the two Cassino sample sets before and after meteorological front (CM03 and CM08, respectively) have not only different concentration level of sulfur but also the size distribution is different. Sulfur is present in sample CM03 dominantly in the fine fraction with modal diameter close to 0.4 μm (typical for urban aerosols), with total concentration of 1350 ± 70 ng/m^3 in PM_9. It means that the combination of May-impactor sampling and TXRF elemental analysis provides realistic results for impactor stages covering the fine fraction. Sample CM08 has much

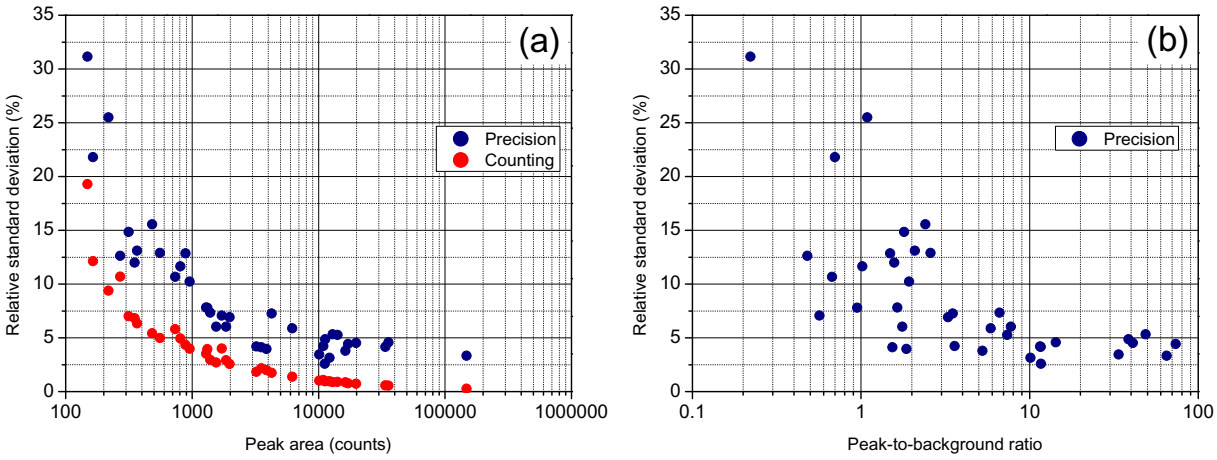

Fig. 1. Repeatability as a function of (a) peak area and (b) peak-to-background ratio.

Table 2
Description and monitoring results of selected samples collected at Cassino and in Budapest. PM_{10} (TEOM), BC (aethalometer at 880 nm) and UVC (BC-equivalent measured by aethalometer at 370 nm) are averages for the sampling periods.

Sample	Location	Date, time	PM_{10} (μg/m^3)	BC (μg/m^3)	UVC (μg/m^3)	Note
CM03	Cassino	21 September 2018 13:07–17:07	17	1.42	1.65	Before cold front
CM08	Cassino	25 September 2018 9:45–15:45	13	0.77	0.88	After cold front
M106	Budapest	01 August 2019 6:00–10:00	12	0.43	0.47	High-sulfate episode
M110	Budapest	02 August 2019 6:00–10:00	29	1.65	1.71	BC and resuspension
M126	Budapest	06 August 2019 6:00–10:00	13	0.95	0.94	High-bromine episode
M134	Budapest	08 August 2019 11:00–15:00	11	0.32	0.37	Elevated lead episode
M137	Budapest	20 August 2019 21:00–22:00	174[a]	n.a.	n.a.	Central fireworks

[a] Erzsébet tér (air quality network station), 300 m from the sampling site.

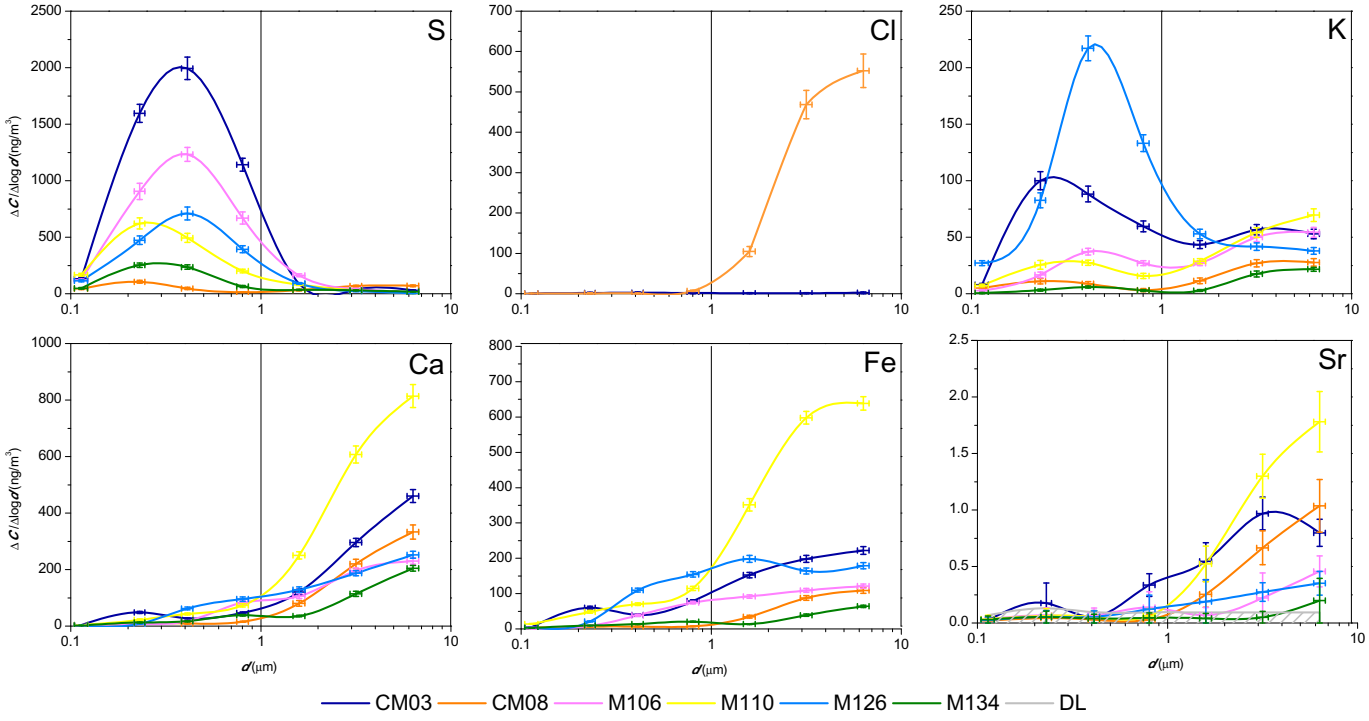

Fig. 2. Size distribution of particulate S, Cl, K, Ca, Fe and Sr concentrations for samples collected in Cassino and Budapest, indicating the respective detection limits for Sr.

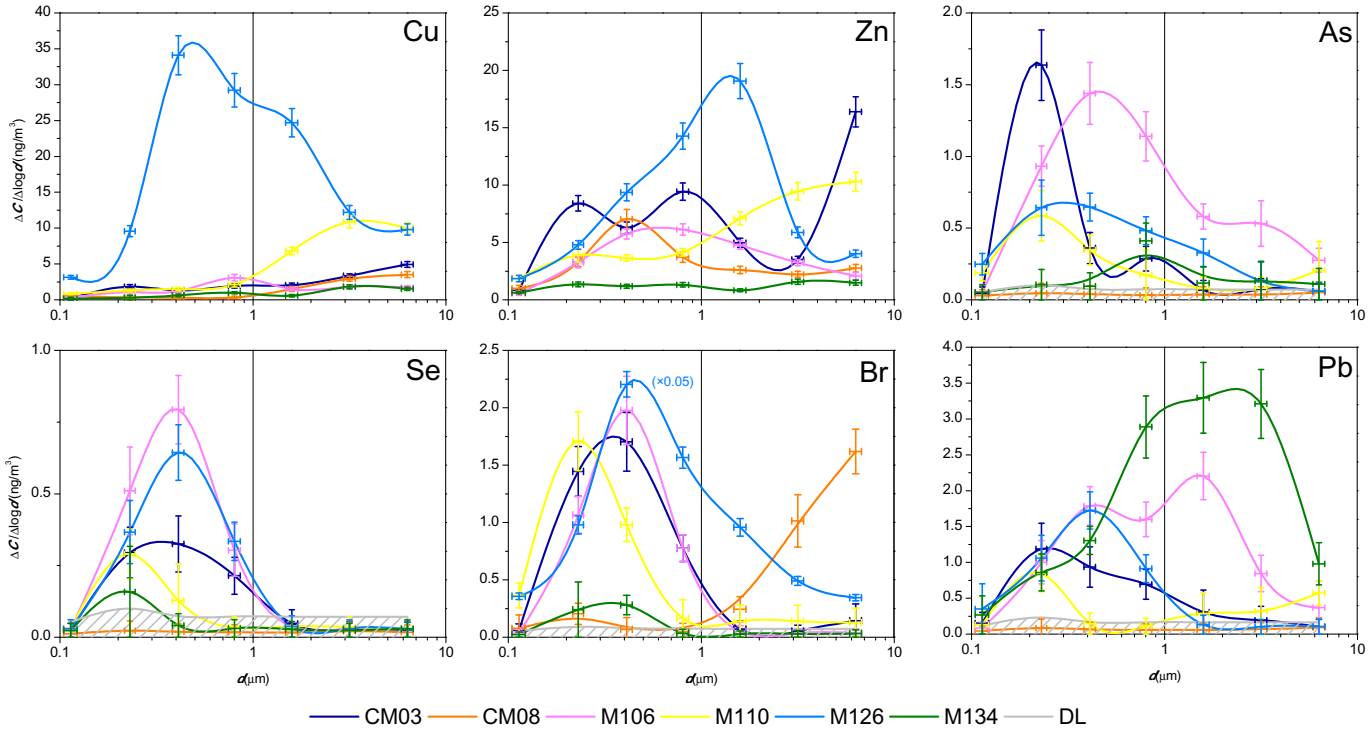

Fig. 3. Size distribution of particulate Cu, Zn, As, Se, Br and Pb concentrations for samples collected in Cassino and Budapest indicating the respective detection limits. Because of the more than 20-fold increase of Br concentrations in the "high bromine" episode, the Br concentrations for sample M126 are multiplied by 0.05 in the plot.

less total concentration of sulfur (110 ± 10 ng/m^3) with a bimodal size distribution. The coarse mode contribution is due to the sea salt aerosol, a different source of sulfate. Sea-salt related sulfate is usually calculated from [SO_4^{2-}]/[Na^+] ratio in seawater [39], [SO_4^{2-}]/[Cl^-] ratio is expected to be higher in sea-salt aerosol than in seawater because of chloride depletion due to reaction with atmospheric reactive gases.

In samples collected in Budapest, sulfur was dominating in the fine fraction (Fig. 2). The modal diameter for samples M106 (sulfate episode, 860 ± 50 ng/m^3 in PM_9) and M126 (bromine episode) was close to that of Cassino samples, around 0.4 μm. The modal diameter was shifted to lower diameters for samples with lower total (PM_9) concentrations, as it was also observed in the literature [40].

Calcium was selected as a major representative element for crustal erosion originated particles expected in the coarse mode having the best statistics in the TXRF spectra. Both samples collected at Cassino (CM03 and CM08) contain Ca in high concentration (300 ± 20 and 200 ± 15 ng/m^3 in PM_9, respectively) with similar size distribution confirming its occurrence in the coarse mode (Fig. 2). Crustal erosion particles are also re-suspended from soil due to traffic in urban areas. The size distribution of Ca concentrations in sample M110 from Budapest related to "BC and resuspension" episode clearly shows that Ca was dominant in the coarse fraction (Fig. 2). The total Ca concentration in PM_9 was the highest, 540 ± 30 ng/m^3. Although there is a major contribution of coarse particles in samples of the other three episodes, smaller peak appears in the submicrometer diameter range below 0.8 μm, which is the most pronounced for the "high-bromine" episode (sample M126). Similar bimodal distributions of Ca were observed in the literature based on IC measurements [40] indicating the presence of Ca sulfate or Ca nitrate in droplet mode.

Since *strontium* can chemically substitute Ca in compounds, its size distribution generally follows the distribution of Ca (see Fig. 2, including DL as well for Sr since concentrations are small, with maximum 1.1 ± 0.2 ng/m^3 in PM_9 for sample M110). The [Sr]/[Ca] ratio in the coarse fraction is similar in Cassino and in Budapest, although it depends on the composition of local soil.

Potassium has a bimodal distribution for all samples studied, the contribution of soil resuspension (coarse mode) and anthropogenic activities (mainly condensation mode) as well (see Fig. 2). Soil-forming aluminosilicate minerals such as clay minerals and feldspars contain potassium at the percentage level. Biogenic particles with K content such as pollens are also dominant in the coarse fraction [41]. Minor amount of K can also be present in secondary ammonium sulfate particles in the condensation mode. Ratio of the two main modes changes for the different pollution episodes. The total K concentration in PM_9 ranges from 16 to 170 ng/m^3 for the selected samples. At Cassino before the meteorological front, the total K concentration in PM_9 was the highest and the condensation mode was dominant in the distribution. Among anthropogenic activities, combustion cannot be excluded since the ratio between UVC and BC as measured by aethalometer was 1.16 (see Table 2) in contrast to 1.00 for morning samples where traffic was the dominant source. After the meteorological front, overall K concentration decreased and the contribution of the coarse mode (soil resuspension) was dominant over the condensation mode. The shape of the potassium size distribution is also very different for the pollution episodes in Budapest. The most striking is the intense peak in the condensation mode around 0.4 μm for the "bromine" event (M126), where the fine fraction dominates in the K concentrations. Sample collected during the other three episodes shows a distribution similar to the Cassino sample after meteorological front, with slight changes of the position of the condensation mode peak, the modal diameter is similar to that of sulfur for each sample.

Iron can originate from diverse natural and anthropogenic sources. According to the measured size distribution (Fig. 2), the highest contribution is in the coarse fraction related to crustal erosion and traffic-generated resuspension as main sources. Similarly to Ca, coarse mode Fe has the highest concentration in traffic-affected pollution episodes at both sites (CM03 and M110). Smaller peaks appear in the fine fraction, mainly in the condensation and in the droplet mode indicating the contribution of anthropogenic sources. The highest contribution in the droplet mode was observed for the "high-bromine" episode (sample

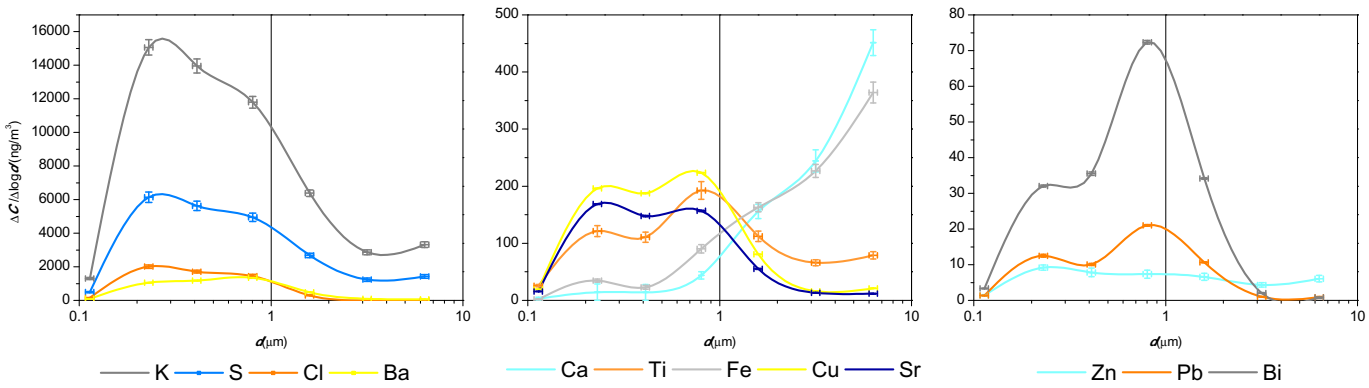

Fig. 4. Size distribution of particulate S, Cl, K, Ca, Ti, Fe, Cu, Zn, Sr, Ba, Pb and Bi concentrations for samples collected in Budapest (Széchenyi tér) during central firework event.

M126).

Among minor and trace elements, *bromine* showed striking differences between the selected samples both in the total PM_9 concentrations and in the size distribution. For Cassino, although the total Br concentration in PM_9 is similar for the two selected samples (around 1 ng/m^3), there is a huge difference in the size distribution (see Fig. 3). While Br in CM03 sampled before the meteorological front was dominating in the fine mode indicating combustion origin, Br had a bimodal distribution in sample CM08 with higher contribution in the coarse mode indicating sea-salt origin. A [Br]/[Cl] ratio of 0.003 was observed in the coarse mode that is close to the value of 0.0035 reported for seawater [42]. Samples collected in Budapest usually contained Br at a concentration level similar to or lower than those collected at Cassino (0.2–1 ng/m^3 in PM_9), dominating in the fine fraction. The modal diameter for Br was observed the same as that of S in all samples. However, a more than 20-times higher Br concentration was observed in a morning sample collected in Budapest (M126), and decreased back to the 1 ng/m^3 level after the event. The modal diameter for the "high-bromine" episode sample was similar to lower Br concentration samples, but the size distribution had a tail towards higher diameters. The possible reason is that condensation of the originally emitted volatile Br could occur onto particles of a wide size range. Most probably Br originated from a local source either from combustion of waste (Br is used as flame retardant in plastics) or temporary use of pesticides in the neighborhood.

It is therefore a highly important result that the combined method of cascade impactor sampling and TXRF analysis can provide realistic size distributions elemental concentrations from short sampling time since short-term pollution episodes can occur with elevated concentrations of specific elements. The detailed study of the elemental size distributions of pollution episodes could lead to a more accurate source apportionment.

Among trace elements, *selenium* shows a unimodal size distribution with modal diameter similar to that of sulfur. Similar unimodal size distributions peaking at around 0.4 μm were reported based on ICP-MS measurements of digested filter samples collected for at least 24 h by cascade impactors at urban areas of Rome and Ferrara (Italy) [13] and Raleigh (NC, USA) [12]. The ratio between Se and S concentrations is different for Cassino and Budapest, but similar for samples collected at the same site, with exception of sample M126 ("bromine" episode). In general, the [Se]/[S] concentration ratio in PM_9 was found as 0.0002 at Cassino and 0.0005 in Budapest. For the "bromine" episode, the ratio was even higher, 0.0008. Although some stages contained Se under the detection limit of TXRF but the size distribution is clearly visible (Fig. 3).

Due to the most typical origin of resuspension and brake wear, the size distribution of *copper* shows a main peak in the coarse fraction [12,13]. The highest contribution of coarse mode Cu was found for sample M110 ("BC and resuspension" episode). However, a high contribution of Cu in the fine fraction was detected for the "bromine" episode (sample M126), with a total concentration in PM_9 3.6 times higher than that of sample M110 (36 vs 10 ng/m^3). The similarity in the size distribution of Cu and Br in sample M126 indicates that the major source of the two elements is the same. Having diverse sources such as metal industry, additive for lubricant in motor vehicles and soil resuspension, *zinc* concentrations usually show a wide size distribution which is different in the studied samples. Similar to Cu, Zn also shows enrichment in the fine fraction for the "bromine" episode (sample M126). For the "traffic" episode in Budapest (sample M110) the Zn distribution shows a bimodal structure similar to that of K (see Figs. 2 and 3), since both end-of-pipe (lubricant additive) and non-end-of-pipe (roadside dust resuspension, tire wear) traffic sources contribute. At Cassino, Zn was found mainly in the fine fraction. At Cassino, *arsenic* and *lead* were mainly found in the fine fraction in the sample collected before the meteorological front (sample CM03), likewise to the results reported for Rome and Ferrara [13]. After the front (sample CM08), the concentrations for both elements were below detection limit of TXRF (Fig. 3). Similarly to other trace elements as Se and Br, there is a main mode of the Pb distribution peaking at 0.3 μm. For the "high sulfate" and "elevated lead" episodes in Budapest (samples M106 and M134, respectively), another peak appeared around 2 μm. The same unimodal and bimodal Pb distributions were observed in cascade impactor samples collected at Raleigh on different days [12]. *Nickel* was found above detection limit only for sample M106 ("high sulfate" episode) stages 7 and 8 (0.18–0.6 μm), indicating a size distribution similar to that of S.

3.2.2. PM related to the central firework in Budapest (20 August 2019)

A sampling as short as 1 h was sufficient for characterizing the elemental size distribution of the firework-related aerosol particles. The sampling location was just 1–5 km away from the places on the shores of the Danube, the Chain Bridge and the ships in the Danube where the fireworks were launched between 21:00 and 21:30. The hourly average PM_{10} mass concentration showed a peak at 22:00 at Erzsébet tér (just 300 m from the sampling site), 174 μg/m^3 being 2.7 times higher than the previous and following hours, and 8 times higher than in the afternoon before or at the night after. Since there are orders of magnitude differences in the elemental concentrations, the size distributions are plotted in three subfigures presenting groups of elements (Fig. 4). K was found to be at the highest concentration level among elements detectable by TXRF (37.5 μg/m^3 in PM_9), followed by S (15.4 μg/m^3), Cl (3.8 μg/m^3) and Ba (3.0 μg/m^3). These values are an order of magnitude higher than 12-24 h averages reported for Girona, Spain [43] and Yanshui, Taiwan [44]. In a recent study of firework festival in Varanasi, India [45], reports a multifold mass increment of firework-specific ions (K^+: 527%; Mg^{2+}: 175%; $NO3^-$: 57%; Cl^-, 291%) in $PM_{2.5}$ aerosol fraction as compared to the background

concentration observed two days before the event.

The main components of fireworks are the fuel (black powder) and the coloring agents. Black powder is a mixture of potassium nitrate, sulfur and organic matter such as charcoal or termite. KNO_3 is used as an oxidizing agent and charcoal (next to sulfur) is the reducing agent. The role of sulfur is to lower the ignition temperature and functions as a reaction speed controller. Coloring agents (strontium, calcium, sodium, barium and copper compounds) are required to achieve the brilliant and colorful nature of fireworks. Chemical elements in the additives provide different flame colors, i.e. red, orange, yellow, yellowish green, green and violet flame colors result from Sr, Ca, Na, Ba, Cu and K, respectively.

The mass distribution of K as measured by TXRF is close to log-normal centered at around 0.4 μm, but wider than detected during a firework event in Göteborg, Sweden [23], meanwhile it shares similarities with the K mass distribution observed in Yanshui, Taiwan [44].

Peak maxima of coloring agents as Sr, Ba are coincident just like in Yanshui [44]. The median of Sr mass distribution takes place around 0.5 μm, which is smaller than that measured in Yanshui [44] but looks similar to the Göteborg sample [23]. Cu, Pb and Bi show similar distribution to Sr, but Bi has a strong maximum at 0.8 μm. The mass distribution of Ti has a slight increase towards the coarse size range indicating that it has a crustal contribution as well. Ca and Fe shows a mass distribution completely different from that of the other elements measured, they are mainly present in the coarse fraction related to soil resuspension (see Fig. 2). Their total PM_9 concentration (670 ng/m^3 for both elements) is not elevated compared to the traffic related samples from the Budapest and Cassino campaigns. Therefore these elements can be considered as non-firework-related, although Ca might be used as flame colorant.

Summing the concentrations for all elements detected by TXRF and added oxygen by stoichiometry, 95 $\mu g/m^3$ of the total mass of PM_9 could be explained. If we consider that additional major elements as C, N, Na, Mg, Al and Si are not detected by TXRF, the explained mass is quite close to the PM_{10} concentration observed at the nearest air quality monitoring station (174 $\mu g/m^3$).

4. Conclusions

The combination of May-impactor sampling and laboratory TXRF analysis provides a simple non-destructive technique to determine mass size distributions of major to trace elements in atmospheric particulate matter. Comparison to literature results using conventional destructive techniques (IC for major ions and ICP-MS/OES for trace elements) demonstrated the acceptable analytical performance and the applicability of the proposed method. The novel technique enables contamination-free sampling and analysis of sub-microgram amounts of particulate matter for major and trace metals as well as S, Cl and Br with high throughput. An optimal size and time resolution can be reached that is harmonized with the analytical capabilities of TXRF and minimizing sample collection artifacts. The possibility of sampling and analysis of large number of size-fractionated samples with 1–4 h collection time is relevant for atmospheric studies where both the sources and the meteorological conditions change in short times. This is principally true for the ultrafine fraction where particle emission, chemical transformation due to aging are vague processes. Elemental mass size distribution provides rich information compared to number size distribution for submicrometer PM even if the technique is not efficient for particles smaller than 70 nm. Moreover, samples collected on Si wafers being semiconductor substrates are readily available for further investigations (Raman, SEM, SRXRF and XAS). It is expected that the on-site use of portable TXRF will extend the in-the-field capabilities of the method, providing fast analytical results for short time pollution episodes.

Declaration of Competing Interest

The authors declare that they have no known competing financial interests or personal relationships that could have appeared to influence the work reported in this paper.

Acknowledgement

This work was supported by European Structural and Investment Funds jointly financed by the European Commission and the Hungarian Government through grant no. VEKOP-2.3.2-16-2016-00011 and by the EMPIR programme co-financed by the Participating States and from the European Union's Horizon 2020 research and innovation programme, through grant agreement 16ENV07 AEROMET.

References

[1] Air quality in Europe, Report 1994-2019, EEA Report, No 10/2019, (2019) (ISSN 1977-8449).
[2] M.G. Perrone, S. Vratolis, E. Georgieva, S. Török, K. Šega, B. Veleva, J. Osán, I. Bešlić, Z. Kertész, D. Pernigotti, K. Eleftheriadis, C.A. Belis, Sources and geographic origin of particulate matter in urban areas of the Danube macro-region: the cases of Zagreb (Croatia), Budapest (Hungary) and Sofia (Bulgaria), Sci. Total Environ. 619–620 (2018) 1515–1529, https://doi.org/10.1016/j.scitotenv.2017.11.092.
[3] S. Breitner, A. Peters, W. Zareba, R. Hampel, D. Oakes, J. Wiltshire, M.W. Frampton, P.K. Hopke, J. Cyrys, M.J. Utell, C. Kane, A. Schneider, D.Q. Rich, Ambient and controlled exposures to particulate air pollution and acute changes in heart rate variability and repolarization, Sci. Rep. 9 (2019) 1946, https://doi.org/10.1038/s41598-019-38531-9.
[4] M.J. Deventer, L. von der Heyden, C. Lamprecht, M. Grause, T. Karle, A. Held, Aerosol particles during the Innsbruck air quality study (INNAQS): fluxes of nucleation to accumulation mode particles in relation to selective urban tracers, Atmos. Environ. 190 (2018) 376–388, https://doi.org/10.1016/j.atmosenv.2018.04.043.
[5] L. Li, Z. Huang, J. Dong, M. Li, W. Gao, H. Nian, Z. Fu, G. Zhang, X. Bi, P. Cheng, Z. Zhou, Real time bipolar time-of-flight mass spectrometer for analyzing single aerosol particles, Int. J. Mass Spectrom. 303 (2011) 118–124, https://doi.org/10.1016/j.ijms.2011.01.017.
[6] H. Wang, L. Shen, Y. Yin, K. Chen, J. Chen, Y. Wang, Characteristics and mixing state of aerosol at the summit of mount tai (1534 m) in central East China: first measurements with SPAMS, Atmos. Environ. 213 (2019) 273–284, https://doi.org/10.1016/j.atmosenv.2019.06.021.
[7] J. Plaza, M. Pujadas, F.J. Gómez-Moreno, M. Sánchez, B. Artíñano, Mass size distributions of soluble sulfate, nitrate and ammonium in the Madrid urban aerosol, Atmos. Environ. 45 (2011) 4966–4976, https://doi.org/10.1016/j.atmosenv.2011.05.075.
[8] I. Grgić, J. Turšič, A. Berner, Applying size segregation to relate the surrounding aerosol pollution to its source, J. Atmos. Chem. 63 (2009) 247–257, https://doi.org/10.1007/s10874-010-9167-9.
[9] A. Ghosh, A. Roy, A. Chatterjee, S.K. Das, S.K. Ghosh, S. Raha, Impact of biomass burning plumes on the size-segregated aerosol chemistry over an urban atmosphere at indo-Gangetic plain, Aerosol Air Qual. Res. 19 (2019) 163–180, https://doi.org/10.4209/aaqr.2017.12.0590.
[10] E. Barbaro, M. Feltracco, D. Cesari, S. Padoan, R. Zangrando, D. Contini, C. Barbante, A. Gambaro, Characterization of the water soluble fraction in ultrafine, fine, and coarse atmospheric aerosol, Sci. Total Environ. 658 (2019) 1423–1439, https://doi.org/10.1016/j.scitotenv.2018.12.298.
[11] H. Rohra, R. Tiwari, P. Khare, A. Taneja, Indoor-outdoor association of particulate matter and bounded elemental composition within coarse, quasi-accumulation and quasi-ultrafine ranges in residential areas of northern India, Sci. Total Environ. 631–632 (2018) 1383–1397, https://doi.org/10.1016/j.scitotenv.2018.03.095.
[12] M.D. Hays, S.-H. Cho, R. Baldauf, J.J. Schauer, M. Shafer, Particle size distributions of metal and non-metal elements in an urban near-highway environment, Atmos. Environ. 45 (2011) 925–934, https://doi.org/10.1016/j.atmosenv.2010.11.010.
[13] G. Simonetti, E. Conte, C. Perrino, S. Canepari, Oxidative potential of size-segregated PM in an urban and an industrial area of Italy, Atmos. Environ. 187 (2018) 292–300, https://doi.org/10.1016/j.atmosenv.2018.05.051.
[14] V. Bernardoni, E. Cucci, G. Calzolai, M. Chiari, F. Lucarelli, D. Massabo, S. Nava, P. Prati, G. Valli, R. Vecchi, ED-XRF set-up for size-segregated aerosol samples analysis, X-Ray Spectrom. 40 (2011) 79–87, https://doi.org/10.1002/xrs.1299.
[15] A. Arana, A.L. Loureiro, H.M.J. Barbosa, R. Van Grieken, P. Artaxo, Optimized energy dispersive X-ray fluorescence analysis of atmospheric aerosols collected at pristine and perturbed Amazon Basin sites, X-Ray Spectrom. 43 (2014) 228–237, https://doi.org/10.1002/xrs.2544.
[16] S. Wang, Q. Yan, R. Zhang, N. Jiang, S. Yin, H. Ye, Size-fractionated particulate elements in an inland city of China: deposition flux in human respiratory, health risks, source apportionment, and dry deposition, Environ. Pollut. 247 (2019) 515–523, https://doi.org/10.1016/j.envpol.2019.01.051.
[17] N. Bukowiecki, P. Lienemann, C.N. Zwicky, M. Furger, A. Richard, G. Falkenberg,

K. Rickers, D. Grolimund, C. Borca, M. Hill, R. Gehrig, U. Baltensperger, X-ray fluorescence spectrometry for high throughput analysis of atmospheric aerosol samples: the benefits of synchrotron X-rays, Spectrochim. Acta B 63 (2008) 929–938, https://doi.org/10.1016/j.sab.2008.05.006.

[18] N. Bukowiecki, P. Lienemann, M. Hill, M. Furger, A. Richard, F. Amato, A.S.H. Prévôt, U. Baltensperger, B. Buchmann, R. Gehrig, PM10 emission factors for non-exhaust particles generated by road traffic in an urban street canyon and along a freeway in Switzerland, Atmos. Environ. 44 (2010) 2330–2340, https://doi.org/10.1016/j.atmosenv.2010.03.039.

[19] S.A. Atwood, J.S. Reid, S.M. Kreidenweis, S.S. Cliff, Y. Zhao, N.-H. Lin, S.-C. Tsay, Y.-C. Chu, D.L. Westphal, Size resolved measurements of springtime aerosol particles over the northern South China Sea, Atmos. Environ. 78 (2013) 134–143, https://doi.org/10.1016/j.atmosenv.2012.11.024.

[20] B.L. Lanzaco, M.L. López, L.E. Olcese, B.M. Toselli, Elemental composition of $PM_{0.25}$ collected in an urban site of Argentina: a first case study, Spectrochim. Acta B 161 (2019) 105712, https://doi.org/10.1016/j.sab.2019.105712.

[21] M. Tahri, M. Bounakhla, M. Zghaid, A. Benchrif, F. Zahry, Y. Noack, F. Benyaich, TXRF characterization and source identification by positive matrix factorization of airborne particulate matter sampled in Kenitra City (Morocco), X-Ray Spectrom. 42 (2013) 284–289, https://doi.org/10.1002/xrs.2484.

[22] A. Wagner, M. Mages, Total-reflection X-ray fluorescence analysis of elements in size-fractionated particulate matter sampled on polycarbonate filters — composition and sources of aerosol particles in Göteborg, Sweden, Spectrochim. Acta B 65 (2010) 471–477, https://doi.org/10.1016/j.sab.2010.02.007.

[23] A. Wagner, J. Boman, M.J. Gatari, Elemental analysis of size-fractionated particulate matter sampled in Göteborg, Sweden, Spectrochim. Acta B 63 (2008) 1426–1431, https://doi.org/10.1016/j.sab.2008.10.010.

[24] J. Prost, A. Zinkl, D. Ingerle, P. Wobrauschek, C. Streli, Evaluation of a sample preparation procedure for total-reflection X-ray fluorescence analysis of directly collected airborne particulate matter samples, Spectrochim. Acta B 147 (2018) 13–20, https://doi.org/10.1016/j.sab.2018.05.005.

[25] J. Prost, P. Wobrauschek, C. Streli, Quantitative total reflection X-ray fluorescence analysis of directly collected aerosol samples, X-Ray Spectrom. 46 (2017) 454–460, https://doi.org/10.1002/xrs.2752.

[26] J. Osán, F. Meirer, V. Groma, S. Török, D. Ingerle, C. Streli, G. Pepponi, Speciation of copper and zinc in size-fractionated atmospheric particulate matter using total reflection mode X-ray absorption near-edge structure spectrometry, Spectrochim. Acta B 65 (2010) 1008–1013, https://doi.org/10.1016/j.sab.2010.11.002.

[27] G. Buonanno, F.C. Fuoco, L. Stabile, Influential parameters on particle exposure of pedestrians in urban microenvironments, Atmos. Environ. 45 (2011) 1434–1443, https://doi.org/10.1016/j.atmosenv.2010.12.015.

[28] K.R. May, An "ultimate" cascade impactor for aerosol assessment, J. Aerosol Sci. 6 (1975) 413–416, https://doi.org/10.1016/0021-8502(75)90057-9.

[29] E. Weingartner, H. Saatho, M. Schnaiter, N. Streit, B. Bitnar, U. Baltensperger, Absorption of light by soot particles: determination of the absorption coefficient by means of aethalometers, J. Aerosol Sci. 34 (2003) 1445–1463, https://doi.org/10.1016/S0021-8502(03)00359-8.

[30] P. Wobrauschek, J. Prost, D. Ingerle, J. Osán, S. Török, C. Streli, Adaption of a TXRF WOBI-module with a low power X-ray tube, 18th International Conference on Total Reflection X-ray Fluorescence Analysis and Related Methods (TXRF-2019), 25–28 June 2019 Girona, Spain.

[31] P. Wobrauschek, P. Kregsamer, C. Streli, H. Aiginger, Instrumental developments in total reflection x-ray fluorescence analysis for K-lines from oxygen to the rare earth elements, X-Ray Spectrom. 20 (1991) 23–28, https://doi.org/10.1002/xrs.1300200106.

[32] C. Streli, P. Wobrauschek, G. Pepponi, N. Zoeger, A new total reflection X-ray fluorescence vacuum chamber with sample changer analysis using a silicon drift detector for chemical analysis, Spectrochim. Acta B 59 (2004) 1199–1203, https://doi.org/10.1016/j.sab.2004.05.007.

[33] P. Wobrauschek, J. Prost, D. Ingerle, P. Kregsamer, N.L. Misra, C. Streli, A novel vacuum spectrometer for total reflection x-ray fluorescence analysis with two exchangeable low power x-ray sources for the analysis of low, medium, and high Z elements in sequence, Rev. Sci. Instrum. 86 (2015) 083105, https://doi.org/10.1063/1.4928499.

[34] B. Vekemans, K. Janssens, L. Vincze, F. Adams, P. Van Espen, Analysis of X-ray spectra by iterative least squares (AXIL): new developments, X-Ray Spectrom. 23 (1994) 278–285, https://doi.org/10.1002/xrs.1300230609.

[35] J. Osán, F. Reinhardt, B. Beckhoff, A.E. Pap, S. Török, Probing patterned wafer structures by means of grazing incidence X-ray fluorescence analysis, ECS Trans. 25 (2009) 441–451, https://doi.org/10.1149/1.3204435.

[36] F. Reinhardt, J. Osán, S. Török, A.E. Pap, M. Kolbe, B. Beckhoff, Reference-free quantification of particle-like surface contaminations by grazing incidence X-ray fluorescence analysis, J. Anal. At. Spectrom. 27 (2012) 248–255, https://doi.org/10.1039/c2ja10286b.

[37] V. Groma, J. Osán, S. Török, F. Meirer, C. Streli, P. Wobrauschek, G. Falkenberg, Trace element analysis of airport related aerosols using SR-TXRF, Időjárás 112 (2008) 83–97.

[38] V.-M. Kerminen, R. Hillamo, K. Teinilä, T. Pakkanen, I. Allegrini, R. Sparapani, Ion balances of size-resolved tropospheric aerosol samples: implications for the acidity and atmospheric processing of aerosols, Atmos. Environ. 35 (2004) 5255–5265, https://doi.org/10.1016/S1352-2310(01)00345-4.

[39] C. Piel, R. Weller, M. Huke, D. Wagenbach, Atmospheric methane sulfonate and non-sea-salt sulfate records at the European project for ice coring in Antarctica (EPICA) deep-drilling site in Dronning Maud land, Antarctica, J. Geophys. Res. 111 (2016) D03304, https://doi.org/10.1029/2005JD006213.

[40] M.A.G. Leiva, R. Toro, R.G.E. Morales, M.A. Ríos, M.R. González, A study of water-soluble inorganic ions in size-segregated aerosols in atmospheric pollution episode, Int. J. Environ. Sci. Technol. 11 (2014) 437–448, https://doi.org/10.1007/s13762-013-0221-4.

[41] A. Worobiec, I. Szalóki, J. Osán, W. Maenhaut, E.A. Stefaniak, R. Van Grieken, Characterisation of Amazon Basin aerosols at the individual particle level by X-ray microanalytical techniques, Atmos. Environ. 41 (2007) 9217–9230, https://doi.org/10.1016/j.atmosenv.2007.07.056.

[42] R. Sander, W.C. Keene, A.A.P. Pszenny, R. Arimoto, G.P. Ayers, E. Baboukas, J.M. Cainey, P.J. Crutzen, R.A. Duce, G. Hönninger, B.J. Huebert, W. Maenhaut, N. Mihalopoulos, V.C. Turekian, R. Van Dingenen, Inorganic bromine in the marine boundary layer: a critical review, Atmos. Chem. Phys. 3 (2003) 1301–1336, https://doi.org/10.5194/acp-3-1301-2003.

[43] T. Moreno, X. Querol, A. Alastuey, F. Amato, J. Pey, M. Pandolfi, N. Kuenzli, L. Bouso, M. Rivera, W. Gibbons, Effect of fireworks events on urban background trace metal aerosol concentrations: is the cocktail worth the show? J. Hazard. Mater. 183 (2010) 945–949, https://doi.org/10.1016/j.jhazmat.2010.07.082.

[44] T.-M. Do, C.-F. Wang, Y.-K. Hsieh, H.-F. Hsieh, Metals present in ambient air before and after a firework festival in Yanshui, Tainan, Taiwan, Aerosol Air Qual. Res. 12 (2012) 981–993, https://doi.org/10.4209/aaqr.2012.03.0069.

[45] S.K. Yadav, M. Kumar, Y. Sharma, P. Shukla, R.S. Singh, T. Banerjee, Temporal evolution of submicron particles during extreme fireworks, Environ. Monit. Assess. 191 (2019) 576, https://doi.org/10.1007/s10661-019-7735-2.